Magnetic Resonance Spectroscopy Artifact Removal by Bayesian Fitting of Complex Voigt Line Shapes

Ludger Starke[1,2]

[1]Berlin Ultrahigh Field Facility, Max Delbrück Center for Molecular Medicine in the Helmholtz Association, Berlin, Germany

[2]Digital Health Center, Hasso Plattner Institute, Potsdam, Germany

Contents

Scope 1
Motivation 2
Model 2
Line shape functions 2
Model parametrization 3
Bayesian estimation 3
Prior information 4
Implementation 4
Baseline subtraction and noise estimation 4
Error function approximation 4
Starting values and fitting algorithm 5
Artifact subtraction and phase correction 5
User Instructions 5
License and Citation 6
References 6

Scope

This repository contains code for the removal of artifact signals from a magnetic resonance (MR) spectrum. The modelled situation consists of two artifact lines and one line originating from the investigated compound. Other signals can be present and should be preserved as long as their frequency does not closely coincide with the artifact peaks. It is expected that there is prior knowledge on the artifact signals in the form of mean and standard deviation values for their frequency, full width at half maximum (FWHM) and Voigt mixing parameter, as well as the relative signal intensity of the two artifact signals. The code can easily be adapted to other applications and we provide an example dataset to enable running a demonstration script.

Motivation

MR spectra are often contaminated with unwanted signals. Most common is a residual water peak from imperfect water suppression in ^{1}H spectroscopy, but also signals from outside the observed object or body and exogenous contaminations can obfuscate the signals of interest. If compounds with short transverse relaxation time T_2^* are investigated, signals originating from components of the radio frequency (RF) array used for RF transmission and signal reception can be detected.

This work was motivated by the study of a fluorinated drug, siponimod, with ^{19}F MR spectroscopy (MRS).[1,2] Siponimod is present in tissues only in very low concentrations and has a ^{19}F-T_2^* below 1 ms. Thus, acquisition methods suitable for detecting siponimod will also pick up traces of ^{19}F-compounds built into the MR hardware. In our case, two distinct artifact lines contaminate the ^{19}F-spectra, despite utilizing a state-of-the art, purpose-built RF array.[3] Please see Starke et al.[2] for details on the experimental setup and the shown example data.

Methods for the removal of nuisance peaks have mostly been developed to handle the residual water peak.[4] These range from simple bandpass filtering to singular value decomposition-based time domain methods.[5] Our application is simpler than removing the residual water peak in that both artifact signals are described well by analytical line shapes. However, it is made challenging by a low signal-to-noise ratio, siponimod signals on the same order of magnitude or even smaller than one of the artifact contributions, and overlapping frequency ranges. Thus, the central consideration during the development of the presented method was achieving stability such that only the unwanted artifact signal is removed and not the siponimod signal itself.

We opted to remove contaminations by directly fitting a superposition of the artifact and true signal peaks to the obtained spectra and then subtracting the artifact contribution. Gaussian priors obtained from control measurements are used to constrain the fit. Most popular MRS fitting tools, such as LCModel,[6] use prior information in the form of model spectra or Bayesian priors. Our contribution is to a) provide an open software environment that can easily be adopted to applications other than single-voxel ^{1}H MRS, and b) fit complex Voigt line shapes in contrast to common frequency domain tools, which only work with the spectra's real part[6-8] or fit a combination of basis spectra.[9] The latter is essential to this application with non-localized spectroscopy, as sample and artifact signals arise from different locations and thus have different phase offsets. It is made feasible by using the error function approximation by Weideman to achieve fast computation times.[10]

Model

Line shape functions

We model the individual spectra as Voigt lines to account for imperfect shimming and susceptibility effects.[11] The Voigt function is approximated by the sum of Lorentzian and Gaussian line shape contributions:

$$V(f, f_c, w, m) = m \cdot L(f, f_c, w) + (1 - m) \cdot G(f, f_c, w), \qquad (1)$$

where V, L and G denote the Voigt, Lorentzian and Gaussian line shape functions, f is the frequency, f_c the center of the peak, w its full width at half maximum (FWHM) and m

controls the mixing of Lorentzian and Gaussian components.[12] Complex Lorentzian and Gaussian lines with unit integral of the real part are given by

$$L(f, f_c, w) = \frac{2/w}{1 + \left(\frac{f - f_c}{w/2}\right)^2} + i \cdot \frac{(f - f_c) \cdot (2/w)^2}{1 + \left(\frac{f - f_c}{w/2}\right)^2} \quad (2)$$

and

$$G(f, f_c, w) = \frac{1}{\frac{w}{2} \cdot \sqrt{\ln 2 \cdot \pi}} \cdot \left(e^{-\left(\frac{f - f_c}{\frac{w}{2} \cdot \sqrt{\ln 2}}\right)^2} + i \cdot \frac{2}{\sqrt{\pi}} \cdot D_+\left(\frac{f - f_c}{\frac{w}{2} \cdot \sqrt{\ln 2}}\right) \right) \quad (3)$$

where D_+ denotes the Dawson function.[12-14]

Model parametrization

Our goal is to model three spectral lines of which two are considered contaminations that should be filtered out. MRS is inherently not a quantitative measurement technique. Thus, knowledge on the absolute artifact amplitudes cannot be transferred between measurements. However, the ratio between the amplitudes of artifact peaks should stay constant and can be constrained using a Bayesian prior. As each line is expected to originate from a different location, we model three individual phase offsets (0^{th}-order phase correction terms). Including a global 1^{st}-order phase term, we arrive at the full line shape

$$\begin{aligned} T(f, \mathbf{a}, r, \mathbf{v}, \mathbf{w}, \mathbf{m}, \boldsymbol{\varphi}, \phi_1) \\ = e^{-i\phi_1 f} \Big(& a_1 e^{-i\varphi_1} V(f, v_1, w_1, m_1) \\ & + a_2 \Big(r\, e^{-i\varphi_2} V(f, v_2, w_2, m_2) \\ & + (1 - r)\, e^{-i\varphi_3} V(f, v_3, w_3, m_3) \Big) \Big), \end{aligned} \quad (4)$$

where vector $\mathbf{a}$ gathers the two amplitudes, r governs the ratio between the artifact peaks, $\mathbf{v}$ collects the peak centers, $\mathbf{w}$ the FWHM values, $\mathbf{m}$ the Voigt mixing parameters, $\boldsymbol{\varphi}$ the 0^{th}-order phases and ϕ_1 is the 1^{st}-order phase correction term. All in all, this line shape model is governed by 16 parameters.

Bayesian estimation

Bayesian techniques allow straightforward inclusion of prior knowledge about the artifact peaks into the estimation of the line shape described by equation (4). Complex MRS data is corrupted by additive Gaussian noise. Describing the prior information also by Gaussian distributions allows for an efficient implementation as a non-linear least squares optimization problem. This choice is appropriate as long as the standard deviation of the Voigt mixing prior is $\ll 1$.

To simplify the presentation, we show Bayesian parameter estimation for a generic model. Consider data $\mathbf{x} = g(\boldsymbol{\theta}) + \boldsymbol{\epsilon}$, $\epsilon_i \sim N(0, \sigma^2)\ \forall\, i$ and thus likelihood function $p(\mathbf{x}|\boldsymbol{\theta}) = N(\mathbf{x}; g(\boldsymbol{\theta}), \sigma^2 I)$. We assume a Gaussian prior distribution over the arguments of function g: $p(\boldsymbol{\theta}) = N\big(\boldsymbol{\theta}; \boldsymbol{\mu}_\theta, \mathrm{diag}(\boldsymbol{\sigma}_\theta^2)\big)$. The posterior over $\boldsymbol{\theta}$ is then $p(\boldsymbol{\theta}|\mathbf{x}) \propto p(\mathbf{x}|\boldsymbol{\theta}) p(\boldsymbol{\theta})$ and, as the Gaussian distribution is its own conjugate prior, will again be a Gaussian distribution such that the maximum a posteriori estimate and posterior mean coincide. It is $\mathrm{argmax}_{\boldsymbol{\theta}}\, p(\boldsymbol{\theta}|\mathbf{x}) = \mathrm{argmax}_{\boldsymbol{\theta}} \ln p(\boldsymbol{\theta}|\mathbf{x}) = \mathrm{argmin}_{\boldsymbol{\theta}} - \ln p(\boldsymbol{\theta}|\mathbf{x})$ and thus

$$\operatorname{argmax}_{\boldsymbol{\theta}} p(\boldsymbol{\theta}|\mathbf{x}) = \operatorname{argmin}_{\boldsymbol{\theta}} \frac{\big(\mathbf{x} - g(\boldsymbol{\theta})\big)^T \big(\mathbf{x} - g(\boldsymbol{\theta})\big)}{\sigma} + \sum_i \left(\frac{(\theta_i - (\boldsymbol{\mu}_\theta)_i)}{(\boldsymbol{\sigma}_\theta)_i} \right)^2 . \quad (5)$$

To map the model of equation (4) onto equation (5), the real and imaginary parts of the complex spectrum are concatenated into one real vector. Bayesian constraints can be omitted on a subset of the parameters by leaving out the respective terms in the summation or letting the corresponding entries of $\boldsymbol{\sigma}_\theta$ go to infinity.

Prior information

For the purpose of this algorithm presentation, it is assumed that means and standard deviations for the artifact frequencies, FWHMs, Voigt mixing parameters and relative signal intensity are already known. In our application, no priors were applied to the parameters of the signal peak, the areas and 0th order phases. Future addition of priors to the signal peak is prepared in the code. The 1st-order phase is softly biased towards 0.

The magnetic field strength in common MR machines drifts by a small amount due to temperature changes and other effects.[15] Additionally, shimming and loading with different samples change the observed resonance frequencies. It was found that it is necessary to account for these effects to avoid a mismatch between experiments. We opted to increase the uncertainty on the artifact line frequencies by what is equivalent to a adding zero-mean Gaussian random variable with a standard deviation of 250 Hz. Appropriate values might change from application to application.

Implementation

Baseline subtraction and noise estimation

A complex baseline is subtracted from the data before fitting the described model. The value is estimated by computing the mean in a manually chosen background region.

It is expected that the spectrum has been smoothed by zero-filling. This can help to achieve a successful fit in low resolution spectra. The resulting noise interpolation needs to be accounted for in the setting of σ such that the balance between data and prior knowledge is not affected. We determine $\tilde{\sigma}$ by computing the standard deviation in the same background region used for baseline estimation and then set $\sigma = \tilde{\sigma} \frac{\text{points after 0-filling}}{\text{measured data points}}$.

Error function approximation

The Dawson function in the imaginary (dispersive) part of the Gaussian line shape function can be defined via the more common error function (erf) or imaginary error function (erfi): $D_+(x) = \frac{\sqrt{\pi}}{2} e^{-x^2} \operatorname{erfi}(x) = -\frac{i\sqrt{\pi}}{2} e^{-x^2} \operatorname{erf}(ix)$.[14] The complex error function is defined via the integral $\operatorname{erf}(z) = \frac{2}{\sqrt{\pi}} \int_0^z e^{-t^2} \mathrm{d}t$ which cannot be stated as a closed-form expression and is thus costly to evaluate. A substantial body of literature has developed for approximations of the error function and its variants.[10,16-18] We chose to implement the approximation of Weideman due to its reliability, computation speed and documentation.[10,19] It should be noted that other modern approximations could be used just as well, e.g. that of Abrarov and Quine.[18]

Weideman develops an approximation of the Fadeeva function $w(z) = e^{-z^2} \cdot (1 - \operatorname{erf}(z))$. The approximation is based on transform $Z = \frac{L+iz}{L-iz}, L \in \mathbb{R}$ and polynomial expansion:

$$w(z) \approx \frac{1}{\sqrt{\pi}(L-iz)} + \frac{2}{(L-iz)^2}\sum_{n=0}^{N-1} a_{n+1} Z^n. \quad (6)$$

The optimal value of L is shown to be $L = 2^{-1/4}N^{1/2}$ and the coefficients a_n are defined via integral $a_n = \frac{L}{\pi}\int_{-\infty}^{\infty} e^{-t^2}\left(\frac{L-it}{L+it}\right)^n \mathrm{d}t$. Weideman demonstrates that this integral can be efficiently approximated by application of the trapezoidal rule, which reduces it to a discrete Fourier transform. For truncation of the polynomial series after 32 coefficients (N=32), the algorithm yields an accuracy of about 12 significant digits. It should be noted that the coefficients a_n only need to be computed once and thus this method is especially suited for the evaluation of vector input. We use $N = 36$ in our code. $w(z)$ relates to the Dawson function by $D_+(x) = -\frac{i\sqrt{\pi}}{2}\left(e^{-x^2} - w(-x)\right)$. Please see the original paper for more detail.[10]

Starting values and fitting algorithm

Where available, the prior means are used as starting values. The user is expected to provide a rough estimate of the signal peak's frequency and width. Manual input is also needed for the 0th-order phase starting values. However, the algorithm was found to be quite tolerant regarding suboptimal settings. For the area starting values, the magnitude spectrum is integrated over the estimated FWHM for each peak. The resulting estimates for the two artifact peaks are summed to yield the starting value of a_2.

To map equation (5) onto a least squares problem, the vectors $(\mathbf{x} - g(\boldsymbol{\theta}))/\sigma$ and $[(\theta_1 - (\boldsymbol{\mu}_\theta)_1)/(\boldsymbol{\sigma}_\theta)_1, \dots]^T$ are concatenated. We use Matlab's build-in `lsqnonlin` function with the trust-region-reflective algorithm, a maximum number of 2000 function evaluations and otherwise standard options.

Artifact subtraction and phase correction

After estimation of the posterior parameter means according to equation (5), these are entered as point estimates into the artifact part of equation (4), which yields the artifact only fit. This line is subtracted from the measured data to yield a cleaned spectrum.

The phase of the remaining peak is determined by fitting a single complex Voigt peak with 0th and 1st-order phase correction with a Bayesian constraint only on the 1st-order term. This was found to be more accurate than using the estimates of the original fit. To avoid local minima, 8 equally spaced phase starting values between 0 and 315 degrees are tested and the phase correction estimate from the fit with the smallest residual are applied to yield the final spectrum.

User Instructions

Download the repository from https://github.com/LudgerS/MRSartifactRemoval. Ensure that both `exampleData.mat` and `priors.mat` as well as the functions folder are on the search path. `Demo.m` runs an evaluation of all described steps for the example dataset. The algorithm's core can be found in function `fitPeakAndCoupledArtifacts.m`.

If you use this code to process your own data, you can repeatedly evaluate section 7 to determine good estimates for the signal peak and phase values. Besides finding these estimates, the code runs fully automatic. If the final phase correction should fail, consider adding more tested phase starting values to avoid any local minima. The following figure shows fit and final output for the example data, which corresponds to the channel 1 data of Kidney M2 from the experiments described in Starke et. al, 2022.[2]

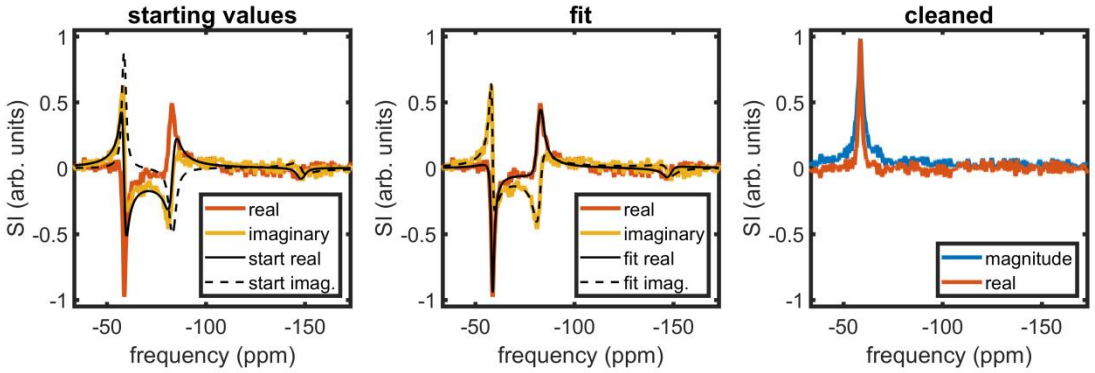

License and Citation

This repository is licensed under GNU GPLv3. If you use this software or the material in this documentation, please cite it according to the output of the repository's citation prompt. Please also cite

> Starke, L. et al. (2022). Detection of Siponimod using Fluorine-19 Magnetic Resonance Imaging. *submitted to Theranostics*

References

1. Cao L, Lao Y, Yao L, et al. Siponimod for multiple sclerosis. *The Cochrane Database of Systematic Reviews.* 2020;2020(6).

2. Starke L, Sherazi F, Prinz C, et al. Detection of Siponimod using Fluorine-19 Magnetic Resonance Imaging. *submitted to Theranostics.* 2022.

3. Waiczies S, Millward JM, Starke L, et al. Enhanced Fluorine-19 MRI Sensitivity using a Cryogenic Radiofrequency Probe: Technical Developments and Ex Vivo Demonstration in a Mouse Model of Neuroinflammation. *Scientific reports.* Aug 29 2017;7(1):9808.

4. Near J, Harris AD, Juchem C, et al. Preprocessing, analysis and quantification in single-voxel magnetic resonance spectroscopy: experts' consensus recommendations. *NMR in biomedicine.* 2021;34(5):e4257.

5. Cabanes E, Confort-Gouny S, Le Fur Y, Simond G, Cozzone P. Optimization of residual water signal removal by HLSVD on simulated short echo time proton MR spectra of the human brain. *Journal of Magnetic Resonance.* 2001;150(2):116-125.

6. Provencher SW. Estimation of metabolite concentrations from localized in vivo proton NMR spectra. *Magnetic resonance in medicine.* 1993;30(6):672-679.

7. Oeltzschner G, Zöllner HJ, Hui SC, et al. Osprey: Open-source processing, reconstruction & estimation of magnetic resonance spectroscopy data. *Journal of neuroscience methods.* 2020;343:108827.

8. Edden RA, Puts NA, Harris AD, Barker PB, Evans CJ. Gannet: A batch-processing tool for the quantitative analysis of gamma-aminobutyric acid–edited MR spectroscopy spectra. *Journal of Magnetic Resonance Imaging.* 2014;40(6):1445-1452.

9. Clarke WT, Stagg CJ, Jbabdi S. FSL-MRS: An end-to-end spectroscopy analysis package. *Magnetic Resonance in Medicine.* 2021;85(6):2950-2964.

10. Weideman JAC. Computation of the complex error function. *SIAM Journal on Numerical Analysis.* 1994;31(5):1497-1518.

11. Marshall I, Bruce SD, Higinbotham J, et al. Choice of spectroscopic lineshape model affects metabolite peak areas and area ratios. *Magnetic resonance in medicine.* 2000;44(4):646-649.

12. Bruce SD, Higinbotham J, Marshall I, Beswick PH. An analytical derivation of a popular approximation of the Voigt function for quantification of NMR spectra. *Journal of Magnetic Resonance.* 2000;142(1):57-63.

13. Keeler J. *Understanding NMR spectroscopy*: John Wiley & Sons; 2011.

14. Wikipedia. Dawson function. 2021; https://en.wikipedia.org/wiki/Dawson_function. Accessed March 27, 2022.

15. Vos SB, Tax CM, Luijten PR, Ourselin S, Leemans A, Froeling M. The importance of correcting for signal drift in diffusion MRI. *Magnetic Resonance in Medicine.* 2017;77(1):285-299.

16. Hart RG. A close approximation related to the error function. *Mathematics of Computation.* 1966;20(96):600-602.

17. Winitzki S. A handy approximation for the error function and its inverse. *A lecture note obtained through private communication.* 2008.

18. Abrarov SM, Quine BM. Efficient algorithmic implementation of the Voigt/complex error function based on exponential series approximation. *Applied Mathematics and Computation.* 2011;218(5):1894-1902.

19. Weideman J. Useful Matlab Files. 1997; http://appliedmaths.sun.ac.za/~weideman/research/matl.html. Accessed March 28, 2022.